THE JOURNAL OF BIOLOGICAL CHEMISTRY VOL. 291, NO. 35, pp. 18410–18418, August 26, 2016

Phosphorylation of Leukotriene C_4 Synthase at Serine 36 Impairs Catalytic Activity*[S]

Received for publication, May 3, 2016, and in revised form, June 14, 2016 Published, JBC Papers in Press, June 30, 2016, DOI 10.1074/jbc.M116.735647

Shabbir Ahmad[‡], A. Jimmy Ytterberg[§¶], Madhuranayaki Thulasingam[‡], Fredrik Tholander[‖], Tomas Bergman[§], Roman Zubarev[§], Anders Wetterholm[‡], Agnes Rinaldo-Matthis[‡], and Jesper Z. Haeggström[‡1]

From the Divisions of [‡]Chemistry II, [§]Chemistry I, and [‖]Biochemistry, Department of Medical Biochemistry and Biophysics, Karolinska Institutet, SE-171 77 Stockholm, Sweden and [¶]Department of Medicine, Solna, Karolinska Institutet, SE-171 76 Stockholm, Sweden

Leukotriene C_4 synthase (LTC4S) catalyzes the formation of the proinflammatory lipid mediator leukotriene C_4 (LTC_4). LTC_4 is the parent molecule of the cysteinyl leukotrienes, which are recognized for their pathogenic role in asthma and allergic diseases. Cellular LTC4S activity is suppressed by PKC-mediated phosphorylation, and recently a downstream p70S6k was shown to play an important role in this process. Here, we identified Ser^{36} as the major p70S6k phosphorylation site, along with a low frequency site at Thr^{40}, using an *in vitro* phosphorylation assay combined with mass spectrometry. The functional consequences of p70S6k phosphorylation were tested with the phosphomimetic mutant S36E, which displayed only about 20% (20 μmol/min/mg) of the activity of WT enzyme (95 μmol/min/mg), whereas the enzyme activity of T40E was not significantly affected. The enzyme activity of S36E increased linearly with increasing LTA_4 concentrations during the steady-state kinetics analysis, indicating poor lipid substrate binding. The Ser^{36} is located in a loop region close to the entrance of the proposed substrate binding pocket. Comparative molecular dynamics indicated that Ser^{36} upon phosphorylation will pull the first luminal loop of LTC4S toward the neighboring subunit of the functional homotrimer, thereby forming hydrogen bonds with Arg^{104} in the adjacent subunit. Because Arg^{104} is a key catalytic residue responsible for stabilization of the glutathione thiolate anion, this phosphorylation-induced interaction leads to a reduction of the catalytic activity. In addition, the positional shift of the loop and its interaction with the neighboring subunit affect active site access. Thus, our mutational and kinetic data, together with molecular simulations, suggest that phosphorylation of Ser^{36} inhibits the catalytic function of LTC4S by interference with the catalytic machinery.

Leukotriene (LT)[2] C_4 synthase (LTC4S) catalyzes the formation of LTC_4 by conjugating the unstable allylic epoxide intermediate LTA_4 with reduced glutathione (GSH) (1). LTC_4 and its metabolites LTD_4 and LTE_4 are known as cysteinyl leukotrienes (cys-LTs), which are involved in bronchial asthma and allergic inflammatory disorders (1–3). The cys-LTs signal through two G-protein-coupled receptors, denoted CysLT1 and CysLT2, to exert their biological functions such as smooth muscle contraction and increased vascular permeability. Several drugs, typified by montelukast, have been developed that specifically target the CysLT1 receptor (4). Recently, additional G-protein-coupled receptors that recognize cys-LTs have been identified, in particular gpr17 and CysLT3 (5, 6). The increasing complexity of cys-LT signaling has promoted research and drug development efforts targeting the upstream LTC4S as it catalyzes the committed step in cys-LT biosynthesis (7).

The leukotrienes are derived from arachidonic acid through the 5-lipoxygenase pathway where cytosolic phospholipase A_2, 5-lipoxygenase, and 5-lipoxygenase-activating protein play important roles (7). Protein phosphorylation/dephosphorylation appear to be important regulatory mechanisms for cellular LT biosynthesis. The two key upstream enzymes, cytosolic phospholipase A_2 and 5-lipoxygenase, are regulated through phosphorylation events, apparently for activation (8) and translocation (9) to the nuclear membrane. LTC4S is yet another enzyme in the 5-lipoxygenase pathway that is regulated by intracellular phosphorylation (10, 11).

LTC4S is an integral membrane protein that belongs to the MAPEG (membrane-associated proteins in eicosanoid and glutathione metabolism) superfamily whose six human members share structural similarity and form homotrimeric enzymes involved in arachidonic acid metabolism and detoxification (12). For 5-lipoxygenase-activating protein, LTC4S, and microsomal prostaglandin E synthase-1, crystal structures have been determined (13–16). Besides LTC4S, no other MAPEG member has been reported to be regulated by phosphorylation. Phosphoregulation of LTC4S was first recognized when protein kinase C (PKC) activation of leukocytes was found to down-regulate LTC4S enzyme activity and attenuate cys-LT production (10). When LTC4S was cloned and sequenced, two putative PKC consensus sites (Ser-Ala-Arg) were found at positions 28 and 111 but were not investigated experimentally (17). In a recent study, it was demonstrated that a ribosomal S6 kinase (p70S6k) is responsible for the observed phosphoregulation of LTC4S in monocytes (18).

* This work was supported in part by Swedish Research Council Grants 10350 and 2301153, Stockholm County Council (Cardiovascular Program), and NovoNordisk Foundation Grant NNF15CC0018346. The authors declare that they have no conflicts of interest with the contents of this article.

The atomic coordinates and structure factors (code 5HV9) have been deposited in the Protein Data Bank (http://wwpdb.org/).

[S] This article contains supplemental Figs. S1–S3 and Tables S1–S3.

[1] Recipient of a distinguished professor award from Karolinska Institutet. To whom correspondence should be addressed. Tel.: 46-8-524-87612 or 46-8-524-87648; Fax: 46-8-736-0439; E-mail: jesper.haeggstrom@ki.se.

[2] The abbreviations used are: LT, leukotriene; DDM, *n*-dodecyl β-D-maltopyranoside; LTA_4, 5(*S*)-*trans*-5,6-oxido-7,9-*trans*-11,14-*cis*-eicosatetraenoic acid; LTC_4, 5(*S*)-hydroxy-6(*R*)-*S*-glutathionyl-7,9-*trans*-11,14-*cis*-eicosatetraenoic acid; LTC4S, leukotriene C_4 synthase; p70S6k, ribosomal S6 kinase; MAPEG, membrane-associated proteins in eicosanoid and glutathione metabolism; cys-LT, cysteinyl leukotriene; MD, molecular dynamics.

The aim of our study was to identify the site(s) on LTC4S that is phosphorylated by p70S6k and investigate the molecular mechanism for suppression of enzyme activity. We identified the sites with an *in vitro* phosphorylation assay, autoradiography, and mass spectrometry. The effects of phosphorylation on enzyme activity and kinetic properties were investigated using LTC4S with phosphorylation-mimicking mutations. To obtain a mechanistic explanation for our experimental results, we analyzed phosphorylated and unphosphorylated forms of LTC4S by comparative molecular dynamics (MD) and determined the crystal structure of the phosphomimetic S36E mutant.

Results and Discussion

Protein phosphorylation constitutes an essential part of the regulation of almost every aspect of cellular function (19). It has previously been shown that LTC4S is also regulated by phosphorylation, and p70S6k was found to be one of the key players in this process (10, 18). The p70S6k is a serine/threonine-specific kinase localized both in the cytosol and nucleus (20). In this study, we show that the predominant p70S6k phosphorylation site on LTC4S is Ser^{36}.

Prediction of Candidate Phosphorylation Site(s)—Initially, we used an online phosphorylation prediction tool, NetPhos 2.0 Server, to identify the potential phosphorylation site(s) based on sequence information using an artificial neural network method (21). The prediction identified six Ser, two Thr, and one Tyr residue (Fig. 1*A*). The major inclusion criteria for further characterization of individual residues were their predictive score and location in the structure. Thus, Ser^{28} and Ser^{36} had the highest probability scores of 0.810 and 0.987, respectively, whereas serine residues at positions 23, 57, 100, and 111 exhibited very low probability scores ranging from 0.002 to 0.159. Because Ser^{23}, Ser^{28}, Ser^{57}, Tyr^{97}, and Ser^{111} are located within the membrane lipid bilayer (Fig. 1, *B* and *C*) with poor accessibility for kinases, we reasoned that the probability that these residues will be phosphorylated is very low. It is common that phosphorylation sites on membrane proteins are located in extramembrane loop regions as in human cardiac Na^+ channel $Na_v1.5$ (22). In LTC4S, Ser^{36} is located in a loop region, and Ser^{100} is found just above the membrane-spanning region within the active site (Fig. 1*C*). The server also predicted two neighboring Thr residues at positions 40 and 41 with relatively high probability scores and located in the same loop as Ser^{36} but with their side chains pointing toward the LTC4S trimer interface (Fig. 1*C*). It should also be noted that a serine/threonine-specific kinase was used for this study, and the relative abundance of the phosphorylated form of Ser, Thr, and Tyr has been reported as a ratio of 1800:200:1 in vertebrate cells (23). Hence, four of nine predicted residues were selected for further analysis, *viz.* Ser^{36}, Ser^{100}, Thr^{40}, and Thr^{41}.

Identification of Phosphorylation Site (s) on LTC4S by MS/MS Analysis—To identify the phosphorylation sites, *in vitro* phosphorylated proteins were analyzed by mass spectrometry. The MS analyses of LTC4S achieved up to 32% sequence coverage. The peptides containing Ser^{36}, Thr^{40}, Thr^{41}, and Ser^{111} could be identified in WT and S36A samples. The peptide covering Ser^{28}, ^{3}DEVALLAAVTLLGVLLQAYFSLQVISAR^{30}, was most likely too large and hydrophobic, whereas the peptide covering

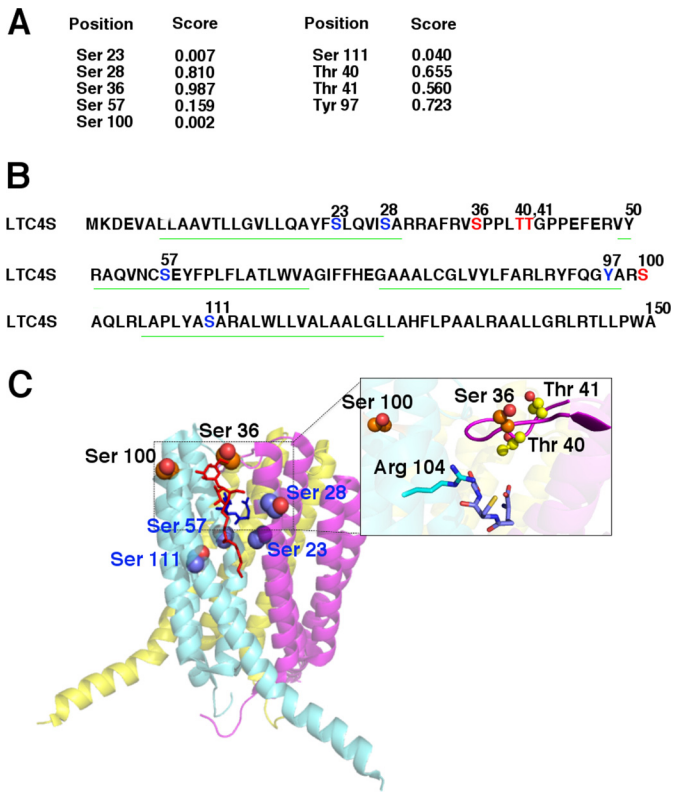

FIGURE 1. **Phosphorylation sites in LTC4S predicted with an online tool, NetPhos 2.0 Server.** *A*, the probability scores for each predicted residue. *B*, the predicted sites are marked in the LTC4S primary structure with the membrane-spanning regions underlined in *green*. Predicted phosphorylation sites located within the membrane are marked in *blue*, and the four residues that were selected for further characterization are marked in *red*. *C*, predicted serine phosphorylation sites are indicated in the LTC4S trimeric structure (Protein Data Bank code 2UUH). DDM, a detergent molecule that is supposed to bind at the same site as LTA_4, is indicated in *red*, and the second substrate GSH is shown in *blue* within the active site. Residues within the membrane-spanning region are labeled in *blue*. A magnified view of the active site of LTC4S within the dimer interface is shown to the *right* in which the DDM molecule has been removed for clarity. The predicted phosphorylation sites (Ser^{36}, Ser^{100}, Thr^{40}, and Thr^{41}) are shown in that region together with the catalytic Arg^{104} and a bound GSH (*blue*) molecule.

Ser^{100}, ^{100}SAQLR^{104}, was too short and hydrophilic. The peptides covering Ser^{36}, Thr^{40}, and Thr^{41}, ^{35}VpSPPLTTGPPEFER^{48} and ^{32}AFRVpSPPLTTGPPEFER^{48} where pS is phosphoserine, were repeatedly found to be phosphorylated. Only singly phosphorylated peptides were detected. In all but two cases, the peptides were phosphorylated at Ser^{36}, and in the other two cases, peptides were phosphorylated at Thr^{40} (Fig. 2), suggesting that Ser^{36} is the predominant phosphorylation site. No evidence was found for phosphorylation of Thr^{41} (supplemental Fig. S1).

To increase the chance of identifying phosphorylation at Ser^{100}, two mutants were used in which the tryptic cleavage site immediately prior to or immediately after the Ser^{100} had been mutated. The R99H was specifically generated for this study, whereas the mutation R104A was published previously (24). MS analyses identified ^{93}YFQGYAHSAQLR^{104} and ^{100}SAQLALAPLYASAR^{113} but only as the non-phosphorylated peptides. Hence, we could not find any mass spectrometric evidence for phosphorylation of Ser^{100}.

Analysis of LTC4S Phosphorylation by Autoradiography—It has been shown previously that LTC4S can be phosphorylated

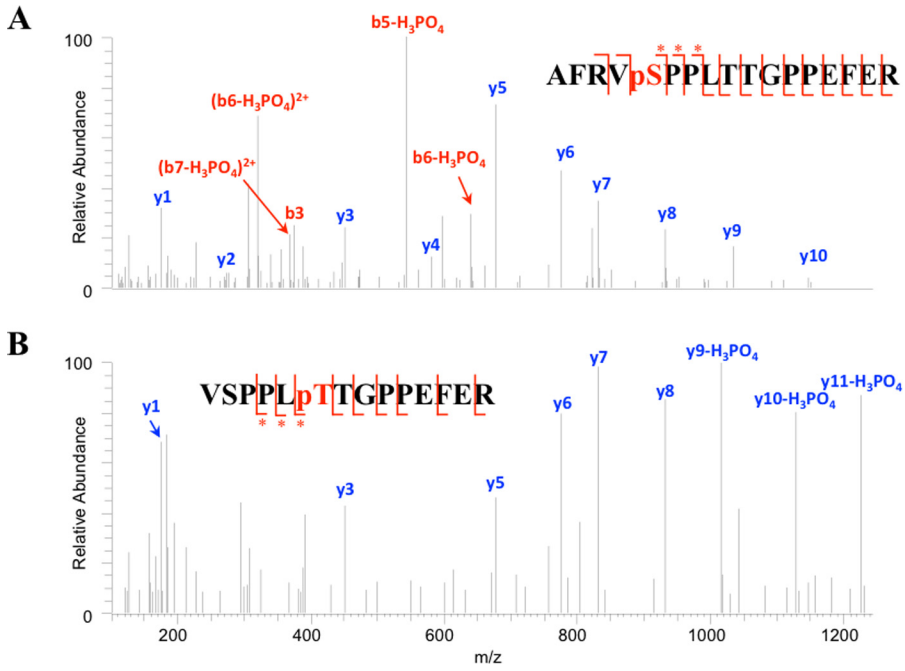

FIGURE 2. **MS/MS (higher energy C-trap dissociation) analysis of phosphorylated LTC4S.** The protein sample was prepared after *in vitro* phosphorylation with p70S6k followed by trypsin digestion. The figure shows the two identified phosphorylation sites. *A*, the annotated MS/MS of the peptide ^{32}AFRVSPPLTTGPPEFER^{48} with the phosphorylation assigned to Ser^{36}. *B*, the annotated MS/MS of the peptide ^{35}VSPPLTTGPPEFER^{48} with the phosphorylation assigned to Thr^{40}. B- and y-ions are indicated (in *red* and *blue*, respectively) together with neutral loss of the phosphate group. *Red bars* in the peptide sequence indicate cleavage of the peptide backbone. Neutral loss is indicated by *. *pS*, phosphoserine; *pT*, phosphothreonine.

in vitro and analyzed by autoradiography. A recombinant p70S6k was used for the *in vitro* phosphorylation assay as described (18). WT LTC4S was incubated with p70S6k in the presence of radioactive [γ-^{32}P]ATP in a reaction mixture as described under "Experimental Procedures." The phosphorylation of LTC4S was found to be detergent-specific. Enzyme purified with Triton X-100 as a detergent displayed a radioactive band with an M_r of about 18,000, corresponding to phosphorylated LTC4S, whereas protein purified with the detergent *n*-dodecyl β-D-maltopyranoside (DDM) was not phosphorylated as judged by the faint radioactive band in the autoradiography (Fig. 3). In the crystal structure of LTC4S, a DDM molecule is bound in an intermonomeric, hydrophobic crevice believed to accommodate the substrate LTA_4 (Protein Data Bank code 2UUH; Fig. 1*C*). Thus, a possible explanation for the prevention of phosphorylation by DDM could be that the detergent molecule blocks the access of the kinases to the phosphorylation site(s). Based on the identification of Ser^{36} as a phosphorylation site in LTC4S, we generated the mutant S36A and incubated it with p70S6k in the presence of radioactive [γ-^{32}P]ATP as with WT LTC4S. However, the results from autoradiography were not consistent and did not provide conclusive evidence to show that S36A mutant was not phosphorylated (data not shown). Thus, a radioactive band was consistently observed that could be due to the presence of an additional site(s), possibly Thr^{40}, as indicated by MS analysis.

The Mutant S36E Displays Significantly Reduced LTC4S Activity—We next investigated the functional consequences of phosphorylation at Ser^{36} by replacing this residue with a Glu (S36E), a common mimic of phosphoserine (25). The effects of mutation on LTC4S activity and kinetic parameters with its physiological substrates LTA_4 and GSH were assessed. Likewise, the mutant T40E was constructed and functionally characterized. The specific activity of S36E LTC4S was reduced by nearly 80% (20 μmol/min/mg) as compared with WT LTC4S (95 μmol/min/mg), whereas for the T40E mutant (67 μmol/min/mg), the activity was reduced by 30% (Fig. 4*A*). The loss of activity of S36E agrees well with the previous observations of down-regulation of LTC4S activity by protein kinases (10, 11). The steady-state kinetic parameters were determined for S36E and T40E mutants using LTA_4 as a substrate to test the effects on substrate binding and catalytic efficiencies (Table 1 and Fig. 4*B*). Interestingly, the catalytic constants k_{cat}^{LTA4} and K_m^{LTA4}

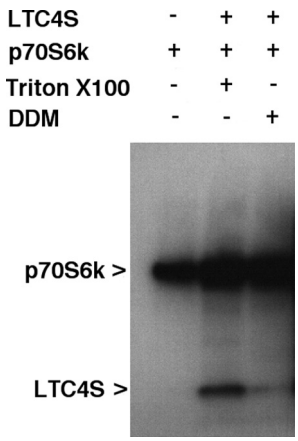

FIGURE 3. **Effect of DDM, a lipid substrate mimic, on the phosphorylation of LTC4S.** Enzyme was subjected to *in vitro* phosphorylation and analyzed by autoradiography as described under "Experimental Procedures." The *first lane* shows the band for p70S6k at around 60 kDa as a control, the *second lane* shows that phosphorylated LTC4S purified using Triton X-100 as the detergent was detected with a size of 18 kDa, and the *third lane* shows that phosphorylation was inhibited when LTC4S was purified with DDM as the detergent.

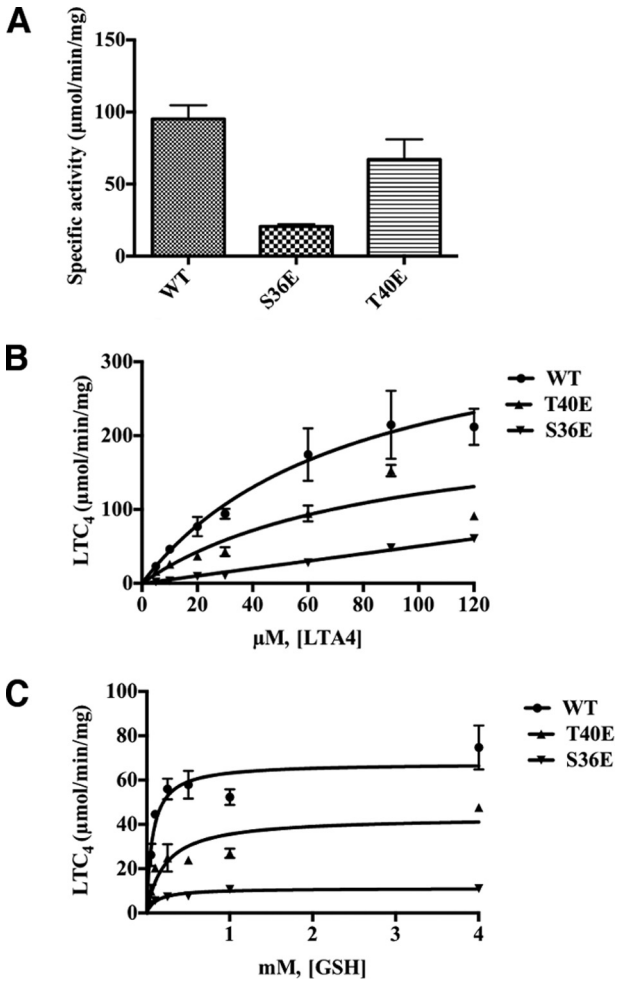

FIGURE 4. **Kinetic properties of WT, S36E, and T40E LTC4S.** *A*, specific activities as determined under "Experimental Procedures." *B*, steady-state kinetics determined with LTA_4 varied between 5 and120 μM while keeping the GSH concentration constant at 5 mM. *C*, steady-state kinetics with GSH concentration varied between 0.05 and 4 mM while keeping the LTA_4 concentration constant at 30 μM. *Error bars* represent S.D.

could not be determined for S36E mutant as the formation of LTC_4 increased linearly with increasing concentrations of LTA_4, indicating that substrate binding is very weak in this mutant. The apparent second order rate constant, k_{cat}/K_m^{LTA4}, which is the effective rate of substrate binding converted to product, was determined as 1.3×10^5 M^{-1} s^{-1}, which is less than 10% of the efficiency displayed by WT LTC4S. In contrast, the catalytic properties of T40E were not changed significantly compared with WT enzyme. Thus, the catalytic turnover at saturating substrate concentration, k_{cat}^{LTA4}, observed for WT and T40E LTC4S was 105 and 62 s^{-1}, respectively, whereas K_m^{LTA4} remained in the same range for WT (76 μM) and T40E (85 μM). Therefore, WT and T40E enzyme displayed catalytic efficiencies, *i.e.* k_{cat}/K_m^{LTA4}, of 13.9×10^5 and 7.7×10^5 M^{-1} s^{-1}, respectively. Together, these data suggest that the active site architecture and enzyme-LTA_4 interactions have been affected due to the introduction of a negative charge at position 36.

The kinetic parameters for the peptide substrate GSH were similar to those of LTA_4 (Table 1). The turnover rate by S36E (k_{cat}^{GSH}) was reduced by 85% (3 ± 0.1 s^{-1}) compared with WT enzyme (19.0 ± 1.0 s^{-1}). The latter value is lower than k_{cat}^{LTA4} due to the lower solubility and stability of LTA_4 compared with that of GSH. The values of K_m^{GSH} for S36E and T40E were a bit higher (120 and 220 μM, respectively) compared with WT enzyme (70 μM) (Table 1). For T40E, the 3-fold increase in K_m^{GSH} may be explained by the results of MD simulations (see below).

Comparative Molecular Dynamics Suggests That a Phosphorylated Ser^{36} Interacts with the Catalytic Arg^{104}—We performed 100-ns molecular dynamics simulations, with snapshots taken every nanosecond, of LTC4S embedded in a lipid bilayer with and without phosphorylation at Ser^{36} (Ser(P)^{36}). Analysis of the simulation snapshots indicated that the simulated systems generally appeared stable with energies and root mean square deviation values stabilizing after ~5 ns of simulation time (supplemental Fig. S2). The largest movements observed were in terminal regions distant from the site of phosphorylation and active site residues and were thus of limited functional relevance.

To identify functionally relevant changes in the motions of LTC4S upon phosphorylation, the dynamic cross-correlation matrix for each simulation was derived (26). To highlight phosphorylation-related differences in correlated movements, the dynamic cross-correlation matrix of native LTC4S was subtracted from the dynamic cross-correlation matrix of phosphorylated LTC4S and plotted as a heat map (supplemental Fig. S3). Two regions stood out in this map: the intersection between the first luminal loop (Arg^{34}–Pro^{43}, including the phosphorylation site) and residues located around the second luminal loop (Ala^{89}–Ala^{110}, including the end of helix 3 and beginning of helix 4) of the neighboring subunit and the intersection between the first luminal loop and residues in the beginning of helix 2 (Pro^{43}–Phe^{60}, *i.e.* right after the first luminal loop) of the neighboring subunit.

The obvious explanation for the changes highlighted by the dynamic cross-correlation matrix analysis is that phosphorylation of Ser^{36} will pull this region toward spatially neighboring residues that provide complementary binding partners. Not all three subunits of LTC4S behaved exactly the same in this aspect, and the cross-subunit contacts were different for the three interfaces. This could be a real difference or just an effect of the limited time span (100 ns) of the simulation, but it is possible that a longer time course would equilibrate all structures at a more uniform state.

A detailed analysis of all simulation snapshots was performed to identify hydrogen bond (H-bond) partners of Ser^{36}/Ser(P)^{36} throughout the simulation time course (supplemental Table S2). The most striking interactions were the H-bonds formed between Ser(P)^{36} and Arg^{104} (Fig. 5) that were present in 15–88% (depending on subunit interface) of all snapshots, which should be compared with <0.4% in the unphosphorylated model (Table 2). This implies a high probability for formation of H-bonds between these residues upon phosphorylation. Importantly, Arg^{104} is the key catalytic residue responsible for formation of the GSH thiolate anion (24). In addition, phosphorylation led to an increased frequency of H-bonding with Arg^{34} in the same subunit. However, because Ser^{36} and Arg^{34} are very close (both spatially and in the primary sequence), this interaction is not likely to have significant functional effects. In

TABLE 1
Steady-state kinetic parameters for phosphomimetic mutants of LTC4S

Enzyme	K_m		k_{cat}		k_{cat}/K_m	
	GSH	LTA_4	GSH	LTA_4	GSH	LTA_4
	μM		s^{-1}		$M^{-1}\,s^{-1}$	
WT	70 ± 18	76 ± 18	19 ± 1.0	105 ± 14	(2.7 ± 0.6) × 10^5	(13.9 ± 1.5) × 10^5
T40E	220 ± 74	85 ± 44	12 ± 1.1	62 ± 18	(0.5 ± 0.1) × 10^5	(7.7 ± 2.0) × 10^5
S36E	120 ± 20	–[a]	3 ± 0.1	–[a]	(0.26 ± 0.03) × 10^5	(1.3 ± 0.03) × 10^5

[a] –, could not be obtained.

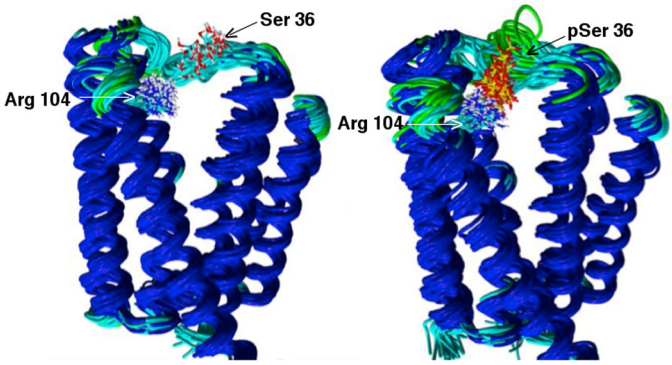

FIGURE 5. **MD simulation of LTC4S and [Ser(P)^{36}]LTC4S.** Shown is a representation of 45 snapshots of MD simulation performed with LTC4S (*left*) and [Ser(P)^{36}]LTC4S (*right*). *Left*, a ribbon representation of subunits A and B with Ser^{36} (*red*) of subunit A and Arg^{104} (*blue*) of subunit B shown for LTC4S. *Right*, the same representation for phosphorylated LTC4S with Ser(P)^{36} (*yellow-red*) of subunit A interacting with Arg^{104} (*blue*) of subunit B.

TABLE 2
Probability of hydrogen bond formation between Ser^{36}/Ser(P)^{36} and Arg^{104} at the three-subunit interfaces during 100 ns of MD

Interface	Probability of H-bond between Ser^{36}/Ser(P)^{36} and Arg^{104}	
	LTC4S + GSH	[Ser(P)^{36}]LTC4S + GSH
	%	
A-B	0.1	87.7
B-C	0.4	17.1
C-A	0	14.5

addition, Arg^{34} is not known to be important for catalysis or substrate binding.

Molecular dynamic simulation was also performed with a phosphorylated Thr^{40} (Thr(P)^{40}) of LTC4S, which revealed a markedly pronounced interaction between Thr(P)^{40} and Arg^{51} of the neighboring subunit (data not shown). Arg^{51} is an anchoring residue for the carboxyl group of the GSH (27) and was found to be not essential for catalysis (24), and its interaction with Thr(P)^{40} may explain the increased K_m^{GSH} of T40E LTC4S as compared with WT enzyme (Table 1).

Crystal Structure of S36E LTC4S—A crystal structure of the mutant S36E was determined at 3-Å resolution (Protein Data Bank code 5HV9; supplemental Table S3), which indicates that the mutant was correctly folded and that the loss of activity is not due to the misfolded protein. The overall structure was similar to native LTC4S (Protein Data Bank code 2UUI) with one monomer in the asymmetric unit. Nine residues (Met^{-5} to Glu^4) and three residues (Pro^{148} to Ala^{150}) were removed in the present structure at the N and C termini, respectively, because of the lack of density. Strong positive density was observed for the thiol group of GSH in the $F_o - F_c$ difference map at 3σ after initial refinement. Contouring $F_o - F_c$ map to 2.5 σ resulted in a positive curved density representing GSH at the active site. The GSH molecule was fitted, and complete density was achieved at 1σ of $2F_o - F_c$ map. A minor positional shift for the thiol group of GSH accompanied by an increased distance (0.7 Å) to Arg^{104} was observed at the active site (Fig. 6) compared with the structure of WT LTC4S with bound GSH (Protein Data Bank code 2UUH), which corroborates the results of MD simulations and provides a structural basis for the reduced catalytic activity displayed by S36E. Moreover, no positive density for a DDM molecule (mimics LTA_4 in 2UUH) was detected in the putative active site of the S36E structure, suggesting that lipid substrate binding is compromised.

Phosphomimetic Mutant S36E Is Less Sensitive to a Synthetic Inhibitor—A recent study suggests that protein phosphorylation may affect drug inhibitor binding to target proteins (28). They classified two types of mechanisms by which phosphorylation affects drug efficacy. In one type, phosphorylation inhibits both drug binding and target activity, whereas in the other type, phosphorylation inhibits drug binding while increasing target activity (28). Here, we used the phosphomimetic mutant S36E to test the effect of phosphorylation on inhibitor binding to LTC4S. In a previous study, a nanomolar inhibitor, TK04, was used to probe the inhibition of human and mouse LTC4S (29). The inhibitor (0.05–15 μM) was incubated with the same amount of WT and S36E enzyme (0.1 μg) at a fixed concentration of LTA_4 (20 μM) and GSH (5 mM). TK04 was less efficient in inhibiting the S36E mutant (IC_{50} = 389 ± 69 nM) at low inhibitor concentrations (≤IC_{50}) compared with WT enzyme (IC_{50} = 211 ± 52 nM), whereas at higher concentrations there were no significant differences (Fig. 7). The observed behavior with the S36E mutant indicates that phosphorylation at Ser^{36} may interfere with TK04 binding, thus effecting the inhibitor potency. TK04 was proposed to occupy the LTA_4 binding site and interact with Arg^{104} based on molecular docking results (30). The efficiency of the TK04 inhibitor at concentrations around or below IC_{50} seems reduced with the phosphomimetic S36E mutant, which is yet an indication that phosphorylation affects lipid substrate binding.

Concluding Remarks—We have used MS/MS analysis and site-directed mutagenesis to identify Ser^{36} as a predominant and functionally important p70S6k phosphorylation site in LTC4S. An alternative site, Thr^{40}, was also identified at low frequency and was found to be of marginal functional relevance. Results of comparative MD simulations and x-ray crystallography indicate that phosphorylation of Ser^{36} acts by disturbing the catalytic action of Arg^{104} and reducing substrate access to the active site (Fig. 8). P70S6k-dependent LTC4S phosphorylation was demonstrated in monocytes (18). Given the complexity of PKC-mediated protein phosphory-

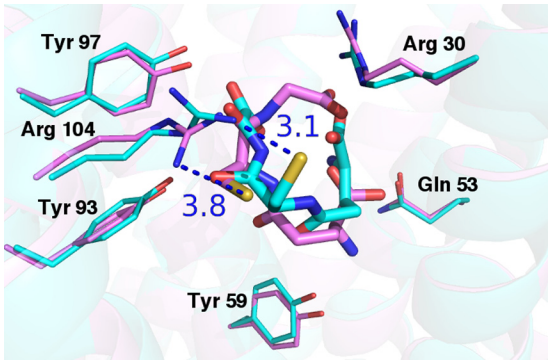

FIGURE 6. **Structure and key residues at the active site of S36E LTC4S.** Superposition of S36E (Protein Data Bank code 5HV9; *magenta*) and WT LTC4S (Protein Data Bank code 2UUH; *cyan*) shows the position of bound GSH within the active site. The distance between the catalytically important residue Arg^{104} and the sulfhydryl group of GSH is increased by 0.7 Å in the S36E structure compared with the WT structure.

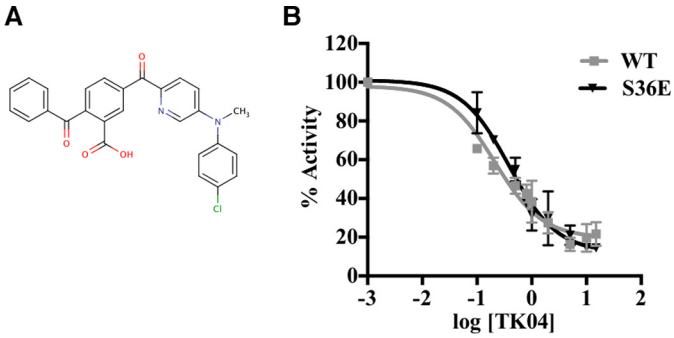

FIGURE 7. **Inhibition studies of WT and S36E LTC4S with an inhibitor, TK04.** *A*, chemical structure of TK04. *B*, dose-response curves showing the inhibition pattern for WT (IC_{50} = 211 ± 52 nM; *gray*), and S36E (IC_{50} = 389 ± 69 nM; *black*) LTC4S by TK04 where 100% activity corresponds to the activity with no inhibitor. Three independent experiments were performed with each data point in triplicate. *Error bars* represent S.E.

lation events, residues other than Ser^{36} may be functional phosphorylation sites involving other kinases in other cellular contexts. Such possibilities deserve further studies and may give additional insights into the mechanisms of LTC4S phosphoregulation.

Experimental Procedures

Chemicals, Reagents, and Enzymes—GSH, 2-mercaptoethanol, imidazole, Tris base, NaCl, Triton X-100, and sodium deoxycholate were obtained from Sigma. DDM was purchased from Anatrace. [γ-^{32}P]ATP was ordered from PerkinElmer Life Sciences. p70S6k, Mg-ATP mixture, and kinase assay dilution buffer were purchased from Merck-Millipore. Pepsin, trypsin, and chymotrypsin were obtained from Promega (Madison, WI). Protease and phosphatase inhibitor mixtures were from Sigma and Thermo Scientific, respectively. LTA_4 was purchased from Cayman as LTA_4 methyl ester and further converted to LTA_4 by saponification as described previously (31).

Site-directed Mutagenesis—Site-directed mutagenesis was performed according to the QuikChange protocol (Stratagene, La Jolla, CA). WT LTC4S cDNA with an additional N-terminal His_6 tag was subcloned into pPICZA (Invitrogen) vector and used as a template to generate all other mutants using the primers listed in supplemental Table S1. To check the mutations and other nonspecific changes, the protein-coding part of the plasmid vectors was verified by DNA sequencing from SEQLAB, Göttingen, Germany.

Protein Expression and Purification—WT LTC4S and all mutants were expressed in yeast *Pichia pastoris*, and the purification was performed in a single step on an *S*-hexylglutathione-agarose column (24). The protein used for the *in vitro* phosphorylation assay was desalted on a PD-10 column to exchange buffer with 20 mM HEPES (pH 7.4) containing 0.1 mM dithiothreitol (DTT) and 0.05% Triton X-100. Conversely, the protein prepared for crystallization was further purified on a Superdex 200 16/60 (GE Healthcare) with 20 mM Tris (pH 8.0), 100 mM NaCl, 0.03% DDM (w/v), and 0.5 mM tris(2-carboxyethyl)phosphine. Protein concentration was determined by the Lowry method (32) or the Pierce™ BCA Protein Assay kit followed by SDS-PAGE on a Phast system (GE Healthcare).

In Vitro Phosphorylation Assay and Autoradiography—The *in vitro* phosphorylation assay was performed as described (18). Briefly, purified LTC4S (2 μg) was incubated with [γ-^{32}P]ATP (0.8 μCi) or 0.5 mM cold ATP premixed in magnesium acetate/ATP mixture (2.5 mM HEPES (pH 7.4), 0.5 mM ATP, and 50 mM magnesium acetate) together with 0.1 μg of p70S6k (T412E; Millipore) in a 5× reaction buffer (20 mM MOPS (pH 7.2), 25 mM β-glycerol phosphate, 5 mM EGTA, 1 mM sodium orthovanadate, and 1 mM DTT; Upstate, Millipore) for 30 min at 30 °C. The proteins were separated using SDS-PAGE and transferred to nitrocellulose membranes. The *in vitro* phosphorylated bands were detected by autoradiography using high performance films (Amersham Biosciences Hyperfilm™ MP, GE Healthcare).

Identification of Phosphorylation Site(s) by Mass Spectrometry—In vitro phosphorylated WT LTC4S was separated using one-dimensional PAGE and stained with Coomassie Brilliant Blue. The protein band was excised manually and digested in gel using a MassPREP robotic protein-handling system (Waters, Millford, MA) according to the manufacturer's instructions. After reduction with DTT and alkylation with iodoacetamide, the proteins were digested with 0.3 μg of trypsin (modified; Promega) in 50 mM ammonium bicarbonate for 5 h at 40 °C. The tryptic peptides were extracted with 1% formic acid and 2% acetonitrile followed by 50% acetonitrile twice. Phosphopeptides were further enriched on a PhosphoCatch™ microspin column (Promega) loaded with a combination of zirconium and titanium oxide resins.

The *in vitro* phosphorylated samples were digested in solution as described previously (33). The proteins were digested overnight in 50 mM ammonium bicarbonate, 30% DMSO, and trypsin (at a ratio of 1:20 trypsin:protein; modified) at 37 °C.

Peptides from both in-gel and in-solution digestion were desalted using ZipTips (C_{18}; Merck Millipore Ltd., Ireland) followed by separation using online nano-scale-LC-MS/MS (reversed phase C_{18}) and analyzed on an LTQ Velos Orbitrap electron transfer dissociation mass spectrometer (Thermo Fisher Scientific, Germany). A 40-min gradient of buffer A and B (A, 0.1% formic acid in water; B, 0.1% formic acid in acetonitrile) was used for the separation as follows: 5–30% B in 35 min followed by 30–95% B in 5 min. The flow rate was 300 nl/min. MS spectra were acquired at a resolution of 60,000 followed by fragmentation of the five most intense peaks. The peptides were

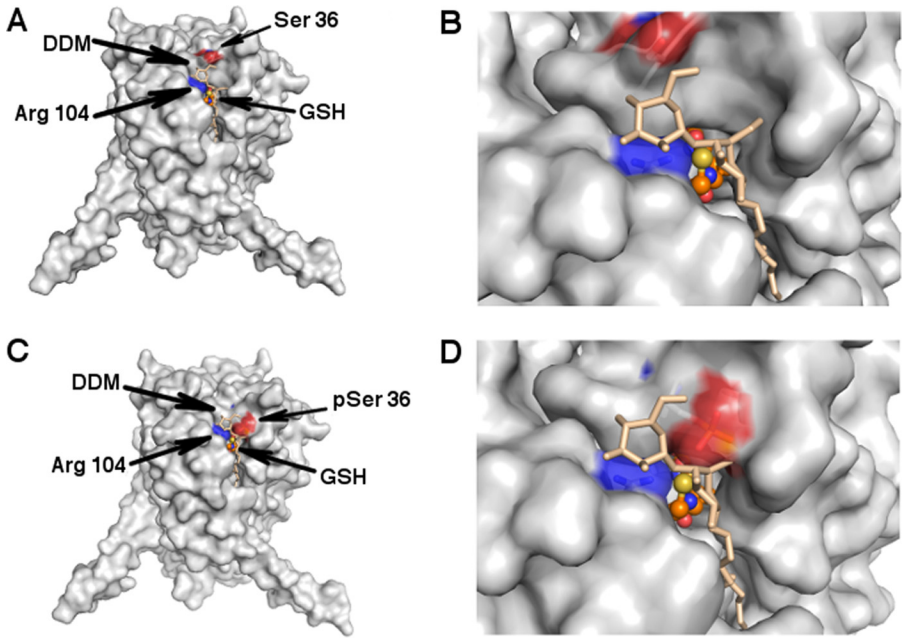

FIGURE 8. **A proposed model of the active site architecture in LTC4S and [Ser(P)^{36}]LTC4S.** *A*, surface representation of the LTC4S trimer and location of the intermonomeric active site cleft (Protein Data Bank code 2UUH). The positions of Ser^{36} (*red*) and catalytically important Arg^{104} (*blue*) together with bound DDM (*wheat*) and GSH are indicated. *B*, a magnification of the hydrophobic substrate-binding crevice with a DDM molecule, Ser^{36}, Arg^{104}, and GSH. *C*, same as in *A* for a model structure of [Ser(P)^{36}]LTC4S displaying the spatial rearrangement of Ser^{36} upon phosphorylation. *D*, same as in *B* for [Ser(P)^{36}]LTC4S. The model structure of [Ser(P)^{36}]LTC4S was generated from the crystal structure of LTC4S (Protein Data Bank code 2UUH) where Ser^{36} was exchanged for phosphoserine in Coot followed by geometry minimization using the PHENIX geometry minimization tool. Finally, the figure was prepared using PyMOL.

either fragmented by only collision-induced dissociation or by higher energy C-trap dissociation first followed by electron transfer dissociation of the same precursor.

Mass lists extracted by Raw2MGF v2.1.3 (34) were searched against the Swiss-Prot database (downloaded February 7, 2014) using Mascot search engine v2.3.02 (Matrix Science Ltd., London, UK). The WT and mutant constructs used in this study were also added to the database. The following parameters were used for the database searching: tryptic digestion (with a maximum of two miscleavages); carbamidomethylation (Cys) as fixed modification; oxidation (Met), pyroglutamate (Gln), deamidation (Asn/Gln), and phosphorylation (Ser/Thr/Tyr) as variable modifications; 10 ppm as precursor tolerance; and 0.25 Da as fragment tolerance.

Enzyme Activity Assay—Formation of the enzyme product LTC_4 was measured by UV absorbance at 280 nm using high performance liquid chromatography (HPLC) as described earlier (24). Enzyme (0.1 μg) together with GSH (5 mM) was incubated in the presence of LTA_4 (30 μM) for 15 s at room temperature in a 100-μl reaction volume and terminated by adding 200 μl of methanol to the reaction mixture followed by the addition of prostaglandin B_2 as an internal standard. The reaction buffer contained 25 mM Tris-HCl (pH 7.8), 0.05% Triton X-100, and 5 mM 2-mercaptoethanol. The steady-state kinetic parameters were determined by varying the LTA_4 concentration from 10 to 120 μM while keeping the GSH concentration at 5 mM. Alternatively, the GSH concentration was varied between 0.05 and 4 mM while the concentration of LTA_4 was kept at 30 μM. The kinetic data were fitted to the Michaelis-Menten equation using non-linear regression in GraphPad Prism to extract all the kinetic parameters. The k_{cat}/K_m was determined using RFFIT in SIMFIT.

Enzyme Inhibition Assay—Inhibition studies of WT and S36E LTC4S with the inhibitor TK04 were performed using an assay in a 96-well format as described earlier (29) to determine the inhibition parameters. The TK04 concentration was varied between 0 and 15 μM while keeping the LTA_4 concentration constant at 20 μM in the presence of 5 mM GSH and 0.1 μg of enzyme. The data were analyzed with non-linear regression using GraphPad Prism to calculate the IC_{50} values.

Molecular Dynamics—For molecular dynamics, the software YASARA Structure was used (35). The crystal structures of human LTC4S with bound GSH (Protein Data Bank code 2UUH with His tag removed and stripped of all water and ligands other than GSH) and with modeled hydrogens in H-bond-optimized positions (36) were used in the simulations. The trimeric form of the enzyme was generated from the information in the Protein Data Bank file. Phosphorylation of Ser^{36} and Thr^{40} was manually built. The AMBER03 force field (37) was used, and force field parameters for non-standard protein residues were generated with YASARA'S built-in AutoSMILES algorithm (38, 39).

By using the default protocol for simulation of membrane proteins in YASARA (YASARA macro for running a molecular dynamics simulation of a membrane protein with normal or fast speed), the protein was embedded in a phosphatidylethanolamine lipid bilayer and slowly adapted (including deletion of clashing protein-membrane residues and energy minimization) to accommodate the inserted protein. Subsequently, water molecules were added, pK_a values were assigned, the whole simulation cell was neutralized by addition of sodium (at locations of lowest electrostatic potential) and chloride (at locations of highest electrostatic potential) ions to a final concentration of 154 mM, and the system was energy-minimized (40).

The final simulation cell extended 15 Å from the protein in the plane of the membrane and 10 Å in the perpendicular direction. The final simulation cell had dimensions of 105.14 × 91.61 × 98.52 Å and contained 432 protein residues, three GSH residues, 266 lipid residues, and 17,908 solvent residues (water, Na^+, and Cl^-).

Simulations were run for 100 ns at constant pressure (1 bar) at 298 K (isothermal-isobaric ensemble), and snapshots were taken every 100 ps. To allow the membrane to equilibrate, water molecules were prevented entry to the lipid bilayer during the initial 250 ps of simulation.

Temperature control was achieved during simulation by a Berendsen thermostat with the scaling factor calculated from the time-averaged temperature (41, 42). For pressure control, the simulation cell was rescaled during simulation using the YASARA option with combined, time-averaged, density and manometer control (41). The integration time step was 4 fs for intermolecular forces and 2 fs for intramolecular forces. Covalent bonds and angles involving hydrogens were constrained using the YASARA version of the LINCS algorithm (41, 43). An 8-Å cutoff was used for van der Waals and long range electrostatic interactions, which were calculated using the particle mesh Ewald method (44).

Crystallization—S36E protein was supplemented with 1 mM GSH and concentrated to 4.5 mg/ml. Crystallization of the mutant was carried out as described (45). Briefly, the concentrated protein was mixed with reservoir solution containing 0.1 M sodium cacodylate (pH 6.5), 0.2 M NaCl, and 2 M ammonium sulfate. The sitting drop vapor diffusion method was performed at room temperature with a protein to reservoir ratio of 1:1. The matured crystals were harvested after 5 days and cryoprotected with reservoir solution containing 15% (v/v) glycerol.

Data Collection and Structure Determination—Cryoprotected S36E crystals were exposed to x-ray for data collection at i04 beam line, Diamond Light Source, UK. 3000 frames were collected with 0.5° oscillation and 20-s exposure per frame. The data set was processed, and reflection output was converted using the XDS package. Molecular replacement was performed using PHASER with WT structure (Protein Data Bank code 2UUI) after removing the coordinates corresponding to heteroatoms. The output coordinates were refined initially with 20 cycles of rigid body refinement followed by restrained refinement in REFMAC. The Coot program was used for model building, and the figures were generated using PyMOL software.

Author Contributions—S. A. performed the experiments and prepared the preliminary version of the manuscript. A. J. Y. performed the MS/MS analysis and contributed to the manuscript. M. T. performed the structure determination and contributed to the manuscript. F. T. performed the MD simulations and contributed to the manuscript. T. B., R. Z., A. W., and A. R.-M. supervised and contributed to the manuscript preparation. J. Z. H. directed the research and contributed to the manuscript. All authors contributed to the analysis of the results and approved the final version of the manuscript.

Acknowledgments—We thank Julia Esser for providing help with the phosphorylation assay, Carina Palmberg for running preliminary MS/MS experiments, and Michaela Mårback for assistance in the kinetic experiments. We thank Diamond Light Source, UK for providing synchrotron radiation facility and assistance at beam line i04.

References

1. Lam, B. K. (2003) Leukotriene C_4 synthase. *Prostaglandins Leukot. Essent. Fatty Acids* **69,** 111–116
2. Austen, K. F. (2008) The cysteinyl leukotrienes: where do they come from? What are they? Where are they going? *Nat. Immunol.* **9,** 113–115
3. Samuelsson, B. (1983) Leukotrienes: mediators of immediate hypersensitivity reactions and inflammation. *Science* **220,** 568–575
4. Drazen, J. M., Israel, E., and O'Byrne, P. M. (1999) Treatment of asthma with drugs modifying the leukotriene pathway. *N. Engl. J. Med.* **340,** 197–206
5. Maekawa, A., Balestrieri, B., Austen, K. F., and Kanaoka, Y. (2009) GPR17 is a negative regulator of the cysteinyl leukotriene 1 receptor response to leukotriene D4. *Proc. Natl. Acad. Sci. U.S.A.* **106,** 11685–11690
6. Kanaoka, Y., Maekawa, A., and Austen, K. F. (2013) Identification of GPR99 protein as a potential third cysteinyl leukotriene receptor with a preference for leukotriene E4 ligand. *J. Biol. Chem.* **288,** 10967–10972
7. Haeggström, J. Z., and Funk, C. D. (2011) Lipoxygenase and leukotriene pathways: biochemistry, biology, and roles in disease. *Chem. Rev.* **111,** 5866–5898
8. Gijón, M. A., Spencer, D. M., Kaiser, A. L., and Leslie, C. C. (1999) Role of phosphorylation sites and the C2 domain in regulation of cytosolic phospholipase A2. *J. Cell Biol.* **145,** 1219–1232
9. Lepley, R. A., Muskardin, D. T., and Fitzpatrick, F. A. (1996) Tyrosine kinase activity modulates catalysis and translocation of cellular 5-lipoxygenase. *J. Biol. Chem.* **271,** 6179–6184
10. Ali, A., Ford-Hutchinson, A. W., and Nicholson, D. W. (1994) Activation of protein kinase C down-regulates leukotriene C4 synthase activity and attenuates cysteinyl leukotriene production in an eosinophilic substrain of HL-60 cells. *J. Immunol.* **153,** 776–788
11. Gupta, N., Nicholson, D. W., and Ford-Hutchinson, A. W. (1999) Demonstration of cell-specific phosphorylation of LTC4 synthase. *FEBS Lett.* **449,** 66–70
12. Jakobsson, P. J., Morgenstern, R., Mancini, J., Ford-Hutchinson, A., and Persson, B. (1999) Common structural features of MAPEG—a widespread superfamily of membrane associated proteins with highly divergent functions in eicosanoid and glutathione metabolism. *Protein Sci.* **8,** 689–692
13. Martinez Molina, D., Wetterholm, A., Kohl, A., McCarthy, A. A., Niegowski, D., Ohlson, E., Hammarberg, T., Eshaghi, S., Haeggström, J. Z., and Nordlund, P. (2007) Structural basis for synthesis of inflammatory mediators by human leukotriene C4 synthase. *Nature* **448,** 613–616
14. Sjögren, T., Nord, J., Ek, M., Johansson, P., Liu, G., and Geschwindner, S. (2013) Crystal structure of microsomal prostaglandin E2 synthase provides insight into diversity in the MAPEG superfamily. *Proc. Natl. Acad. Sci. U.S.A.* **110,** 3806–3811
15. Ferguson, A. D., McKeever, B. M., Xu, S., Wisniewski, D., Miller, D. K., Yamin, T. T., Spencer, R. H., Chu, L., Ujjainwalla, F., Cunningham, B. R., Evans, J. F., and Becker, J. W. (2007) Crystal structure of inhibitor-bound human 5-lipoxygenase-activating protein. *Science* **317,** 510–512
16. Ago, H., Kanaoka, Y., Irikura, D., Lam, B. K., Shimamura, T., Austen, K. F., and Miyano, M. (2007) Crystal structure of a human membrane protein involved in cysteinyl leukotriene biosynthesis. *Nature* **448,** 609–612
17. Lam, B. K., Penrose, J. F., Freeman, G. J., and Austen, K. F. (1994) Expression cloning of a cDNA for human leukotriene C4 synthase, an integral membrane protein conjugating reduced glutathione to leukotriene A4. *Proc. Natl. Acad. Sci. U.S.A.* **91,** 7663–7667
18. Esser, J., Gehrmann, U., Salvado, M. D., Wetterholm, A., Haeggström, J. Z., Samuelsson, B., Gabrielsson, S., Scheynius, A., and Rådmark, O. (2011) Zymosan suppresses leukotriene C_4 synthase activity in differentiating monocytes: antagonism by aspirin and protein kinase inhibitors. *FASEB J.* **25,** 1417–1427
19. Cohen, P. (2002) The origins of protein phosphorylation. *Nat. Cell Biol.* **4,** E127–E130
20. Fleckenstein, D. S., Dirks, W. G., Drexler, H. G., and Quentmeier, H. (2003) Tumor necrosis factor receptor-associated factor (TRAF) 4 is a new binding partner for the p70S6 serine/threonine kinase. *Leuk. Res.* **27,** 687–694
21. Blom, N., Gammeltoft, S., and Brunak, S. (1999) Sequence and structure-

based prediction of eukaryotic protein phosphorylation sites. *J. Mol. Biol.* **294,** 1351–1362
22. Marionneau, C., and Abriel, H. (2015) Regulation of the cardiac Na^+ channel NaV1.5 by post-translational modifications. *J. Mol. Cell. Cardiol.* **82,** 36–47
23. Mann, M., Ong, S. E., Grønborg, M., Steen, H., Jensen, O. N., and Pandey, A. (2002) Analysis of protein phosphorylation using mass spectrometry: deciphering the phosphoproteome. *Trends Biotechnol.* **20,** 261–268
24. Rinaldo-Matthis, A., Wetterholm, A., Martinez Molina, D., Holm, J., Niegowski, D., Ohlson, E., Nordlund, P., Morgenstern, R., and Haeggström, J. Z. (2010) Arginine 104 is a key catalytic residue in leukotriene C4 synthase. *J. Biol. Chem.* **285,** 40771–40776
25. McSorley, T., Ort, S., Hazra, S., Lavie, A., and Konrad, M. (2008) Mimicking phosphorylation of Ser-74 on human deoxycytidine kinase selectively increases catalytic activity for dC and dC analogues. *FEBS Lett.* **582,** 720–724
26. Ichiye, T., and Karplus, M. (1991) Collective motions in proteins: a covariance analysis of atomic fluctuations in molecular dynamics and normal mode simulations. *Proteins* **11,** 205–217
27. Rinaldo-Matthis, A., Ahmad, S., Wetterholm, A., Lachmann, P., Morgenstern, R., and Haeggström, J. Z. (2012) Pre-steady-state kinetic characterization of thiolate anion formation in human leukotriene C_4 synthase. *Biochemistry* **51,** 848–856
28. Smith, K. P., Gifford, K. M., Waitzman, J. S., and Rice, S. E. (2015) Survey of phosphorylation near drug binding sites in the Protein Data Bank (PDB) and their effects. *Proteins* **83,** 25–36
29. Niegowski, D., Kleinschmidt, T., Ahmad, S., Qureshi, A. A., Mårback, M., Rinaldo-Matthis, A., and Haeggström, J. Z. (2014) Structure and inhibition of mouse leukotriene C4 synthase. *PLoS One* **9,** e96763
30. Kleinschmidt, T. K., Haraldsson, M., Basavarajappa, D., Lundeberg, E., Thulasingam, M., Ekoff, M., Fauland, A., Lehmann, C., Kahnt, A. S., Lindbom, L., and Haeggström, J. Z. (2015) Tandem benzophenone amino pyridines, potent and selective inhibitors of human leukotriene C4 synthase. *J. Pharmacol. Exp. Ther.* **355,** 108–116
31. Wetterholm, A., Medina, J. F., Rådmark, O., Shapiro, R., Haeggström, J. Z., Vallee, B. L., and Samuelsson, B. (1991) Recombinant mouse leukotriene A4 hydrolase: a zinc metalloenzyme with dual enzymatic activities. *Biochim. Biophys. Acta* **1080,** 96–102
32. Lowry, O. H., Rosebrough, N. J., Farr, A. L., and Randall, R. J. (1951) Protein measurement with the Folin phenol reagent. *J. Biol. Chem.* **193,** 265–275
33. Ytterberg, A. J., Peltier, J. B., and van Wijk, K. J. (2006) Protein profiling of plastoglobules in chloroplasts and chromoplasts. A surprising site for differential accumulation of metabolic enzymes. *Plant Physiol.* **140,** 984–997
34. Lyutvinskiy, Y., Yang, H., Rutishauser, D., and Zubarev, R. A. (2013) In silico instrumental response correction improves precision of label-free proteomics and accuracy of proteomics-based predictive models. *Mol. Cell. Proteomics* **12,** 2324–2331
35. Krieger, E., Darden, T., Nabuurs, S. B., Finkelstein, A., and Vriend, G. (2004) Making optimal use of empirical energy functions: force-field parameterization in crystal space. *Proteins* **57,** 678–683
36. Krieger, E., Dunbrack, R. L., Jr., Hooft, R. W., and Krieger, B. (2012) Assignment of protonation states in proteins and ligands: combining pK_a prediction with hydrogen bonding network optimization. *Methods Mol. Biol.* **819,** 405–421
37. Duan, Y., Wu, C., Chowdhury, S., Lee, M. C., Xiong, G., Zhang, W., Yang, R., Cieplak, P., Luo, R., Lee, T., Caldwell, J., Wang, J., and Kollman, P. (2003) A point-charge force field for molecular mechanics simulations of proteins based on condensed-phase quantum mechanical calculations. *J. Comput. Chem.* **24,** 1999–2012
38. Wang, J., Wolf, R. M., Caldwell, J. W., Kollman, P. A., and Case, D. A. (2004) Development and testing of a general amber force field. *J. Comput. Chem.* **25,** 1157–1174
39. Jakalian, A., Jack, D. B., and Bayly, C. I. (2002) Fast, efficient generation of high-quality atomic charges. AM1-BCC model: II. Parameterization and validation. *J. Comput. Chem.* **23,** 1623–1641
40. Krieger, E., Nielsen, J. E., Spronk, C. A., and Vriend, G. (2006) Fast empirical pK_a prediction by Ewald summation. *J. Mol. Graph. Model.* **25,** 481–486
41. Krieger, E., and Vriend, G. (2015) New ways to boost molecular dynamics simulations. *J. Comput. Chem.* **36,** 996–1007
42. Berendsen, H. J. C., Postma, J. P. M., Van Gunsteren, W. F., DiNola, A., and Haak, J. R. (1984) Molecular dynamics with coupling to an external bath. *J. Chem. Phys.* **81,** 3684–3690
43. Hess, B., Bekker, H., Berendsen, H. J. C., and Fraaije, J. G. E. M. (1997) LINCS: a linear constraint solver for molecular simulations. *J. Comput. Chem.* **18,** 1463–1472
44. Essmann, U., Perera, L., Berkowitz, M. L., Darden, T., Lee, H., and Pedersen, L. G. (1995) A smooth particle mesh Ewald method. *J. Chem. Phys.* **103,** 8577–8593
45. Niegowski, D., Kleinschmidt, T., Olsson, U., Ahmad, S., Rinaldo-Matthis, A., and Haeggström, J. Z. (2014) Crystal structures of leukotriene C4 synthase in complex with product analogs: implications for the enzyme mechanism. *J. Biol. Chem.* **289,** 5199–5207